Extreme thunderstorm ground enhancements registered on Aragats in 2023

A. Chilingarian[ORCID], B. Sargsyan, T. Karapetyan[ORCID], D. Aslanyan[ORCID], S. Chilingaryan[ORCID], L. Kozliner, and Y. Khanikyanc

A. Alikhanyan National Lab (Yerevan Physics Institute), Yerevan 0036, Armenia

In 2023, a series of intense thunderstorm ground enhancements (TGEs) were recorded on Mount Aragats in Armenia, with seven events exceeding the fair-weather cosmic ray flux by more than 75%. This study comprehensively analyzes these TGEs, investigating the atmospheric conditions and electric fields contributing to their occurrence. Key insights include discovering relationships between TGE electron content and the location of atmospheric electric fields, recovering electron and gamma-ray energy spectra, and the impact of the cloud charge structure. The findings offer a deeper understanding of TGEs' role in atmospheric physics and its synergy with high-energy astrophysics.

I. INTRODUCTION

In 2023, 56 intense thunderstorm ground enhancements (TGEs, [1,2]) were observed on Mount Aragats, Armenia. The largest of these, marked by dramatic tenfold increases in cosmic ray fluxes compared to fair-weather conditions, was observed on May 23 [3,4]. This study delves into the atmospheric processes driving these phenomena, shedding light on the generation of high-energy particles during thunderstorms.

TGEs are initiated when the electric field within thunderclouds surpasses a critical threshold, accelerating free atmospheric electrons. This process, known as relativistic runaway electron avalanches [5], results in the multiplication of energetic electrons, producing bremsstrahlung gamma rays. These gamma rays can further interact through photonuclear reactions to generate neutrons [6], contributing to the complex mixture of particles observed during a TGE event.

The dynamic structure of thunderclouds plays a pivotal role in TGE development [7,8]. Specifically, the formation of charged layers within the clouds—such as the main negatively and positively charged layers (MN and MP) and induced by MN mirror charge in the Earth (MIRR1), along with an additional lower positively charged region (LPCR) and its mirror (MIRR2)—creates electron and positron accelerated (decelerated) dipoles. These dipoles undergo continuous changes, altering the modes of particle acceleration as the cloud's charge structure evolves.

Over the past decade, Mount Aragats and other sites like Mount Lomnicky Stit, Zugspitze, and Mount Musala have documented nearly a thousand TGE events, with some showing cosmic ray flux enhancements up to 100 times the background levels [9].

However, till now, only TGEs observed by the Aragats Space Environmental Center (ASEC, [10]) have entered the databases accompanied by measurements done by field meters, weather stations, and all-sky cameras [11,12]. The intensities and energy spectra of TGE electrons, gamma rays, and neutrons are measured by approximately 100 channels of particle detectors.

We categorize TGEs based on their characteristics—the flux enhancement relative to fair-weather values, duration, electron and gamma-ray energy spectra, presence of lightning flashes abruptly terminating TGEs, stability of the flux, and unique TGEs coincide with observable optical glows registered by all-sky cameras [13]. One of the most important tasks is understanding the vertical and horizontal extent of the electric field supporting TGE development.

The experimental efforts on Mount Aragats are integral to uncovering the enigmatic high-energy physics within atmospheric plasmas (HEPA, [14]). Comprehending these phenomena enhances our understanding of natural particle acceleration mechanisms within Earth's atmosphere and space plasmas, thus offering broader implications for atmospheric science and astrophysical research.

II. INSTRUMENTATION

Below are briefly described the instruments used in 2023 to measure neutral and charged particle fluxes, near-surface electric field (NSEF), lightning location, skies above Aragats, and meteorological parameters. Time series from all facilities are entered via radio modems to the MySQL database at the headquarters of the Cosmic Ray Division of

Yerevan Physics Institute (CRD) in Yerevan. Data in graphical and numerical format are available online via the ADEI data analysis platform [15], which combines multivariate visualization and statistical analysis. The ADEI data analysis platform allows for multivariate visualization and correlation analysis of time series collected during 15 years of operation.

Experimental facilities are located inside and around three experimental halls on Aragats [16]. In the MAKET experimental hall is located the Aragats Solar Neutron Telescope (ASNT, data available from 2003), which remains the largest spectrometer in HEPA research (4 m^2), measuring the flux of electrons and gamma rays in the energy range 10–100 MeV. In the same hall are the Aragats Neutron Monitor (ArNM, data from 2003), type 18HM64, SEVAN particle detector (data from 2008), and muon detector (data from 2012)—sixteen plastic scintillators of the MAKET-ANI surface array record both EASs and TGEs. The electric field sensor, DAVIS weather station, and all-sky camera are installed on the roof of the MAKET building.

A network of three STAND1 detectors is located at Aragats station premises covering a 50000 m^2 area; see Fig. 1. STAND1 modules are placed at the vertices of a triangle with lengths of 137, 226, and 240 m. The STAND1 detector consists of three layers of 1 cm thick, 1 m^2 area scintillators stacked vertically. Additionally, the same-type 3 cm thick plastic scintillator stands apart. The scintillator's light is reradiated into the long-wavelength region of the spectrum by the spectrum-shifter fibers and transmitted to the photomultiplier (PMT, FEU 115 M). The STAND1 detector is adjusted by changing the high voltage applied to the PMT and setting the shaper-discriminator thresholds.

FIG. 1.   STAND1 particle detector network at Aragats research station, 3200 m above sea level.

The discrimination level is chosen to ensure high signal detection efficiency and maximum suppression of photomultiplier noise. Based on simulations and calibration experiments, we estimate the efficiency of the STAND1 upper scintillator for charged particles to be more than 95%, with energy thresholds of around 1 MeV. We use eight digital inputs from three National Instrument's MyRio boards [4] to feed signals from the STAND1 network and EFM 100 electric mill. Each MyRio board generates an output signal that includes the 50 ms count rates from four scintillators, near-surface electric field value, and the GPS timestamp of the trigger signal. This way, the count rates and NSEF strengths measured by STAND1 and EFM 100 networks are synchronized on a millisecond time scale. The NSEF is continuously monitored by a network of commercially available field mills (Model EFM-100, [17]), three of which are placed at the Aragats station, one at the Nor Amberd station at a distance of 12.8 km from Aragats, one in Burakan village, 15 km from Aragats, and one in Yerevan, at a distance of 39.1 km from Aragats. Sensors were calibrated at the fair-weather in the same location. The distances between the three field mills at Aragats are 80, 270, and 290 m. The sensitivity distance of EFM-100 for the lightning location is 33 km, and the response time of the instrument is 100 ms. The electrostatic field changes are recorded at a frequency of 20 Hz. Data on the continuous monitoring of the NSEF field starting from 2010 (1 sec time series) are available via ADEI.

Meteorological conditions are measured by Vantage Pro2 Plus automatic weather stations from Davis Instruments [18]. The stations include a rain collector, temperature and humidity sensors, an anemometer, a solar radiation sensor, and a UV sensor. They are in Aragats (2 units), Nor Amberd, Burakan, and Yerevan.

The ALLSKY CAM panoramic cameras from Moonglow Technologies produce 24/7 monitoring of the skies above Aragats station. A one-minute time series of camera shots is available directly from the ADEI menu (from 2012). A circular fisheye system provides a 190° hemispherical field of view. The image sensor is a Color 1/3" Sony Super HAD CCD II with an effective pixel number across FoV of 546×457, with an automatic exposure time (from 10^{-5} to 4 sec). In 2018, two additional cameras were installed on the roof of new small laboratory houses an electric mill and weather station. The new laboratory is intended to host instruments from other parties for calibrating their airborne particle detectors with TGEs registered by Aragats facilities. We use cameras for observing transient luminous events coinciding with large TGEs, and the graupel falls by the characteristic specks on the camera glass.

A network of seven spectrometers (based on NaI crystals of $12 \times 12 \times 28$ cm size) are installed in the SKL experimental hall. The low energy threshold spectrometers (∼300 keV) provide large statistics (∼50000 counts per

minute) for recovering the TGE differential energy spectrum [19]. In the same hall is located a STAND3 detector, which comprises four layers of 3 cm thick, 1 m^2 sensitive-area scintillators stacked vertically. Four stacked scintillators of STAND3 have energy thresholds for detecting electrons approximately 5, 20, 30, and 40 MeV and are used to estimate the electron content of TGE by measuring the four scintillators' coincidences. The coincidence "1000" isolates electrons and gamma rays with energies above 5 MeV, while, for instance, "1110" targets electrons above 30 MeV with very small gamma-ray contamination. Electrons with lower energies are absorbed within the detector's body.

The energy spectra were recovered from the measured energy release histograms by the CUBE detector, detailed in [20]. We use two 20 cm thick and 0.25 m^2 area plastic scintillators for spectrometry and a 1 cm thick and 1 m^2 area scintillator fully covering spectrometric scintillators for separating charged and neutral fluxes. The methodology of spectra recovery was the same as for the ASNT spectrometer [19].

Under the west wall of the SKL building operates another STAND1 module. Lightning discharges' wideband electric field waveforms are recorded with a circular flat-plate antenna followed by a passive integrator. The output of the integrator is connected via a 60 cm double-shielded coaxial cable to a Picoscope 5244B digitizing oscilloscope. The frequency bandwidth of the wideband electric field measuring system is 50 Hz to 12 MHz (the RC decay time constant was 3 ms). The record length is 1 sec, including 200 ms prerigger time and 800 ms post-trigger time. The sampling rate is 25 MS/s (sampling interval of 40 ns), and the amplitude resolution is 8-bit. The fast wideband electric field data from 2014 are stored on the CRD servers and available upon request.

The third STAND1 detector and electric mill are located at the roof GAMMA calorimeter of the ANI experiment [21]. In the underground hall, a 200 m^2 muon detector is located, by which the maximum energy of solar proton accelerators was estimated to be above 20 GeV (Solar energetic event of January 20, 2005, [22]).

III. CONTINUOUS MONITORING OF ELECTRIC FIELDS AND PARTICLE FLUXES ON MOUNT ARAGATS

In 2023, 56 TGEs were registered by particle detectors [3]. This number is well above the 11-year TGE mean of 35.5. The lowest number of registered TGEs was in 2019, with 15 registrations; in 2024, till September, there were no TGEs registered with enhancement above 20%. The count rate of 7 TGEs exceeds 75%, and five exceeds 100% above the fair-weather value measured by the STAND3 detector [23]. The strongest May 23 TGE intensity exceeded the fair-weather intensity tenfold (by the STAND1 network upper scintillator). The fluence of the longest TGE on May 27 reaches 38 particles/cm^2 (with energies above 1 MeV). The largest TGEs sustain a very stable flux for a few minutes, demonstrating the astonishing stability of atmospheric electron accelerators.

Figure 2 shows 1-minute time series measurements of particle fluxes, NSEF, and distances to lightning flashes over 2023. Intense thunderstorms on Aragats, as seen in Fig. 2, primarily concentrated in May–July, when the NSEF reached and overpassed $+/-30$ kV/m. NSEF in fine weather is ≈ 0.15 kV/m. The 24/7 monitoring of NSEF by the network of BOLTEK's EFM 100 electric mills on Aragats offers crucial insights into rapid electrification
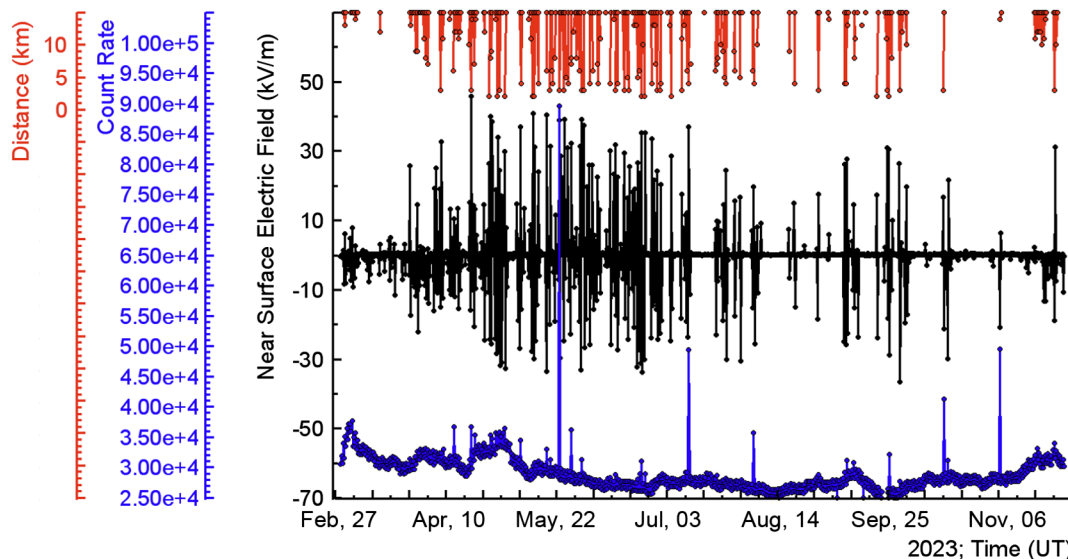

FIG. 2. The black curve shows disturbances of the NSEF measured by the EFM 100 electric field sensor; the blue curve shows a time series of 1-minute count rates of STAND3 upper scintillator ("1000" coincidence, signal only in the upper scintillator); the lines red shows distances to lightning flashes.
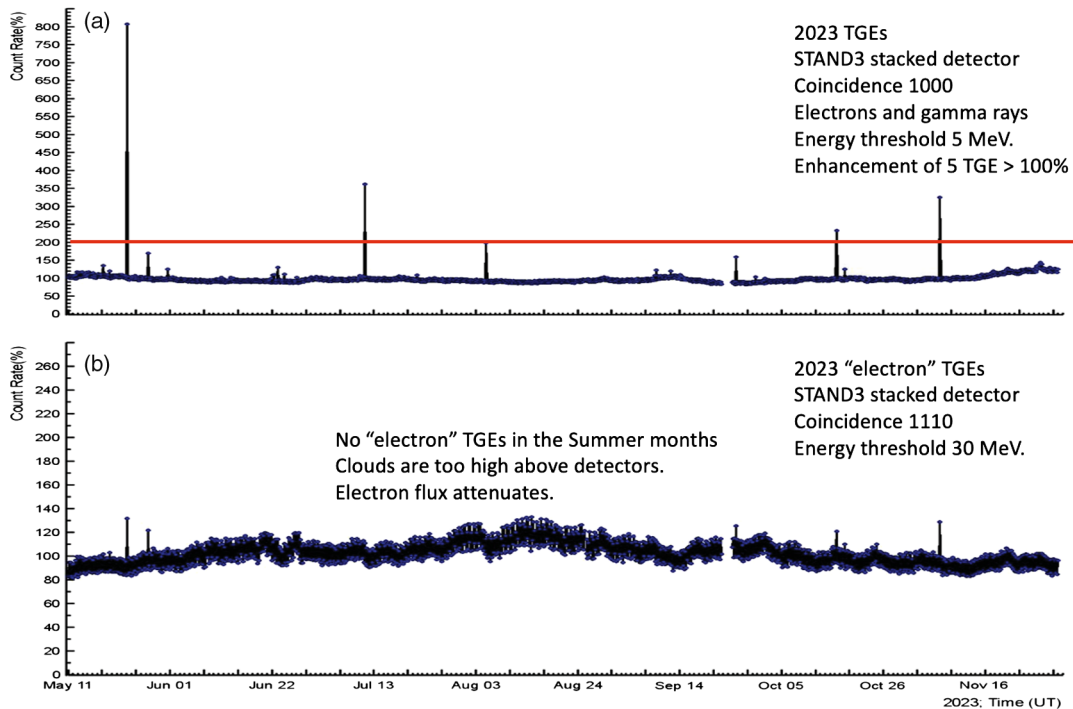
FIG. 3. (a) TGE events occurred on Aragats from May to November 2023—1-minute time series of the STAND3 detector. The "1000" coincidence selects low-energy electrons and gamma rays; (b) the "1110" coincidence selects high-energy electrons (> 30 MeV).

changes in the lower atmosphere. The most significant advantages of NSEF monitoring include its ability to reveal the cloud charge structure in the lower atmosphere directly associated with emerging dipoles in thunderclouds. The blue curve in Fig. 2 depicts a 1-minute time series of count rate; TGEs are indicated by sharp lines above the background. Red lines in Fig. 2 indicate nearby lightning flashes.

Five TGE events surpass the limit of 100% enhancement (by STAND3's "1000" coincidence), shown above the red line in Fig. 3(a). The huge TGE of May 23 ($\approx$800% enhancement) is the largest among $\approx$700 TGEs during the HEPA research started in 2008 on Aragats.

The largest "electron TGEs," targeting electrons with energies above 30 MeV, occurred on May 23 and November 6, as shown in Fig. 3(b). A significantly higher number of high-energy electrons were detected at the peak flux on these dates compared to other large TGEs. There is a wide range of particle fluxes, NSEF strengths, and atmospheric conditions during TGEs, with no two TGEs exhibiting the same relationships. Identifying causal relationships among TGEs, AEF, lightning occurrences, and weather parameters is challenging.

We do not measure the atmospheric electric field and wind speed at the altitudes where the electron accelerator operates. Instead, we use proxies: NSEF and near-surface wind. AEF and wind speed can be much larger at these altitudes than NSEF and surface wind. To address this limitation, we need to send UAVs with appropriate sensors

to the skies to measure these parameters directly and develop new models of RREA dynamics. We plan to do this next year. Meanwhile, multivariate correlation analysis can help uncover useful relationships between measurements.

IV. DETAILED DESCRIPTION OF THE LARGEST TGES

In Fig. 4, we present four of the seven largest summer and autumn TGEs registered by the upper scintillators of the STAND1 network depicted in Fig. 1. There is a difference in the count rate rise and decay in summer [Figs. 4(a) and 4(b)] and autumn TGEs [Figs. 4(c) and 4(d)]. Summer TGEs are highly uniform; in the autumn TGEs, we see asymmetry between detectors located at a distance $\approx$ of 100 m at the highland near Kari Lake (red and blue curves) and remote detector located $\approx$250 m lower on the slope of the mountain opened to the Ararat Valley. Previously, we detected asymmetry of the near-surface electric field (NSEF) measured at these locations by the electric field sensors [13].

Despite the variations in the count rate enhancements of the three modules shown in Fig. 4, the particle flux is consistent across an area of approximately 50000 square meters covered by the STAND1 network. The locations of the detectors can explain variations in the flux enhancement. STAND1, situated on the roof of GAMMA, is exposed from all sides, whereas the building walls partially obstruct the other two detectors. In previous studies [24], we reported TGEs recorded at the Aragats and Nor Amberd research stations within a few minutes, which
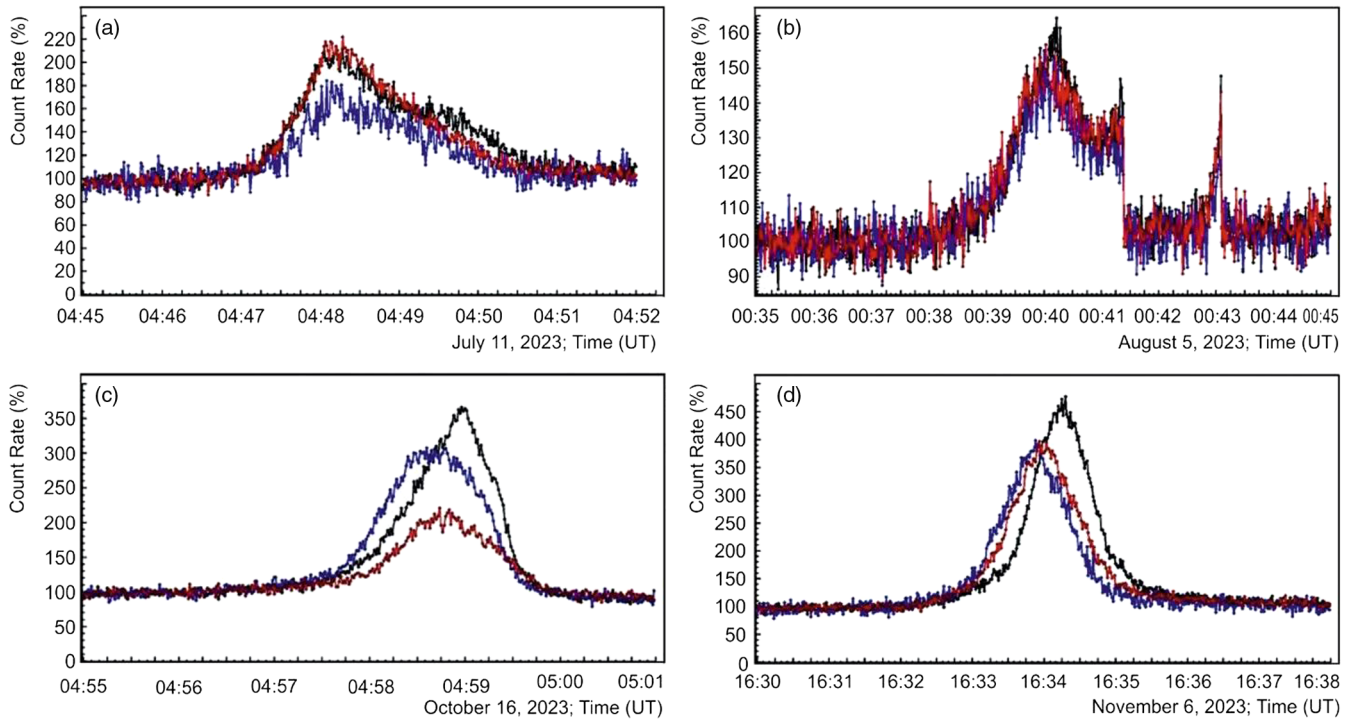
FIG. 4.   One-second time series of count rates of upper scintillators of the STAND1 network. Black—STAND1 unit on the roof of GAMMA experimental hall; blue—nearby MAKET, and red—nearby SKL experimental halls. (a) July 11, (b) August 5, (c) October 16, and (d) November 6.

are 13 kilometers apart. A significant mesoscale electric field over both stations covers several cubic kilometers in the atmosphere. This is causing particle fluxes to reach the Earth's surface over several square kilometers. The radiation emitted by the upper dipole also indicates a permanent large-scale electric field and large-scale gamma radiation detected by airborne gamma detectors. The Airborne Lightning Observatory (ALOFT), flying above the violent thunderstorms in the equatorial regions, registered hundreds of gamma-ray bursts with duration from microseconds to minutes [25]. Electron accelerators operate across a vast area of the upper and lower atmosphere, and symmetric runaway avalanches are developing over large areas, extending towards open space and the Earth's surface.

Figure 5 shows the time series of count rate (blue curve), along with disturbances of NSEF (black curve) and distances to the lightning flash (red lines). We present in Fig. 5 the largest TGE of 2023, which occurred on May 23, Fig. 5(a). Count rates are measured by the upper scintillator of the STAND1 network located on the roof of the GAMMA experimental hall.

There are distinctions in the NSEF-TGE relation in different seasons. The spring TGE [Fig. 5(a)] started at a small positive NSEF, quickly turning negative. TGE flux rises with enhancing negative NSEF till abruptly terminated by lightning flash. The TGE in summer [Fig. 5(b)] occurred during a positive NSEF, first decreasing smoothly to the negative domain and then quickly turning positive at the TGE

flux rise. After being in the positive domain for a few minutes, NSEF turns to the negative domain and stays there until TGE smoothly ends. Afterward, in 5 min, two nearby flashes were detected. Minimal lightning activity was present during autumn TGEs, which displayed symmetric and smooth bell-like shapes. Both TGEs occurred during negative NSEF. TGE on October 16 started at a small positive NSEF, which smoothly decreased and reached -25 kV/m at maximum flux [Fig. 5(c)]. During the TGE on November 6 [Fig. 5(d)], a remote flash (14 km) coincides with an abrupt decrease of NSEF and the start of TGE. Thus, despite the shapes and durations of TGEs being close, the relation to NSEF (a proxy of the AEF) is very different. Since TGEs occur at both positive and negative NSEF, cloud accelerators operate in different fast-changing modes, accelerating electrons and decelerating positrons, and vice versa, accelerating positrons and decelerating electrons depending on the height of emerging charge structures [26,27]. Lightning flashes terminate particle fluxes at different phases of TGE development. For more detail, see our classification of the lightning types terminating TGEs [28,29].

To gain further insight into TGEs, we investigate the stability of the particle flux at its maximum values. Figure 6 compares the 50 ms time series of TGE count rates with the time series measured at the same time the day before during fair weather. TGE time series are well above the fair-weather ones. In the legends, we present the selected intervals of TGE (from 30 sec to 1 min), count rate means,
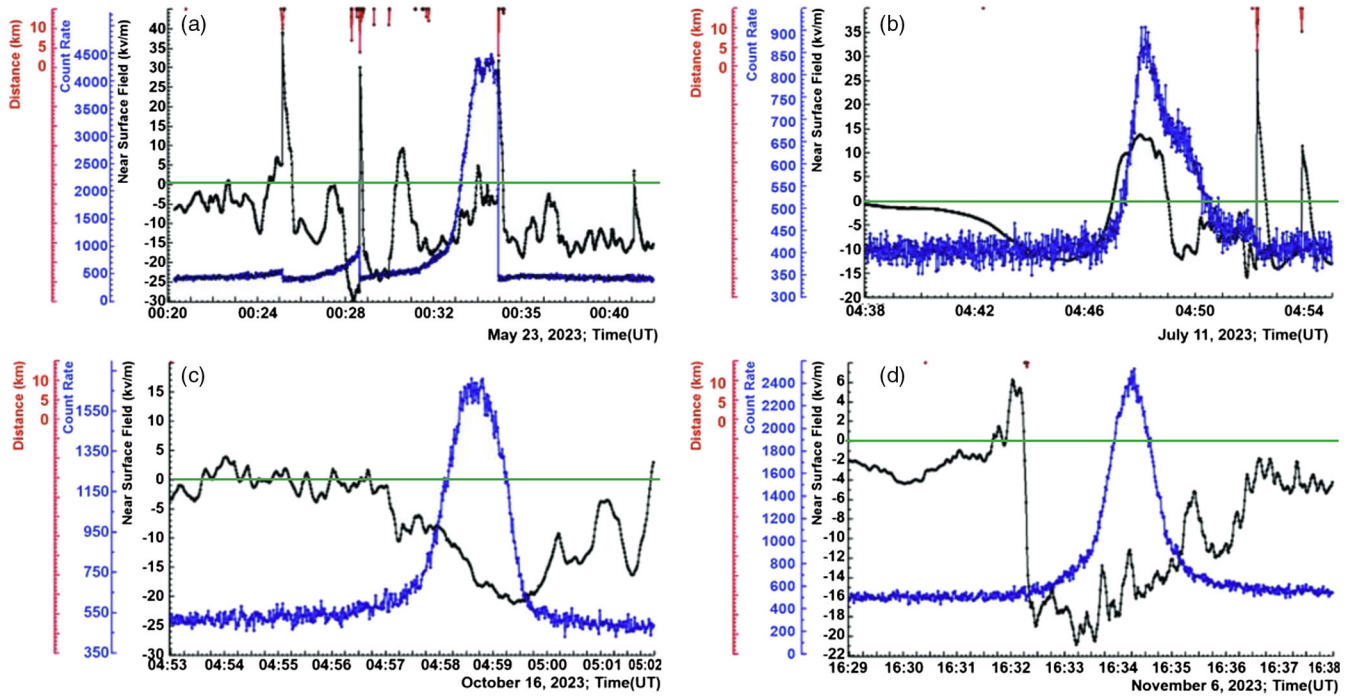
FIG. 5. Black curves—disturbances of NSEF measured by the EFM 100 sensors. Blue curves—1-minute time series of count rates of STAND3 detector (signal only in the upper scintillator). Red—distances to the lightning flash. The green horizontal lines show the zero NSEF. (a) May 23, (b) July 11, (c) October 16, and (d) November 6.
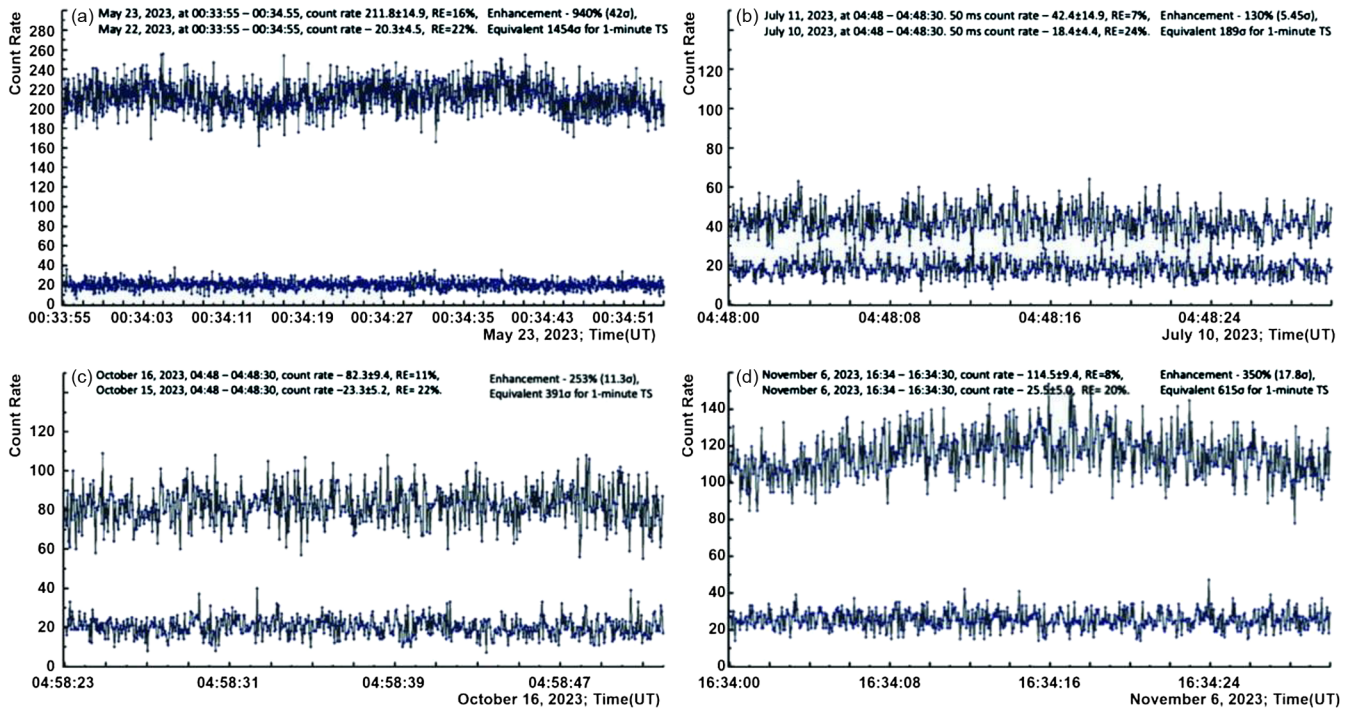

FIG. 6. 50 ms time series of count rates of the STAND1 detector's upper scintillator (GAMMA). The lower curve in each frame corresponds to the count rate measured in fair weather at the same time one day before TGE. The legend includes each TGE's mean count rates, standard errors, and significances. (a) May 23, (b) July 11, (c) October 16, and (d) November 6.
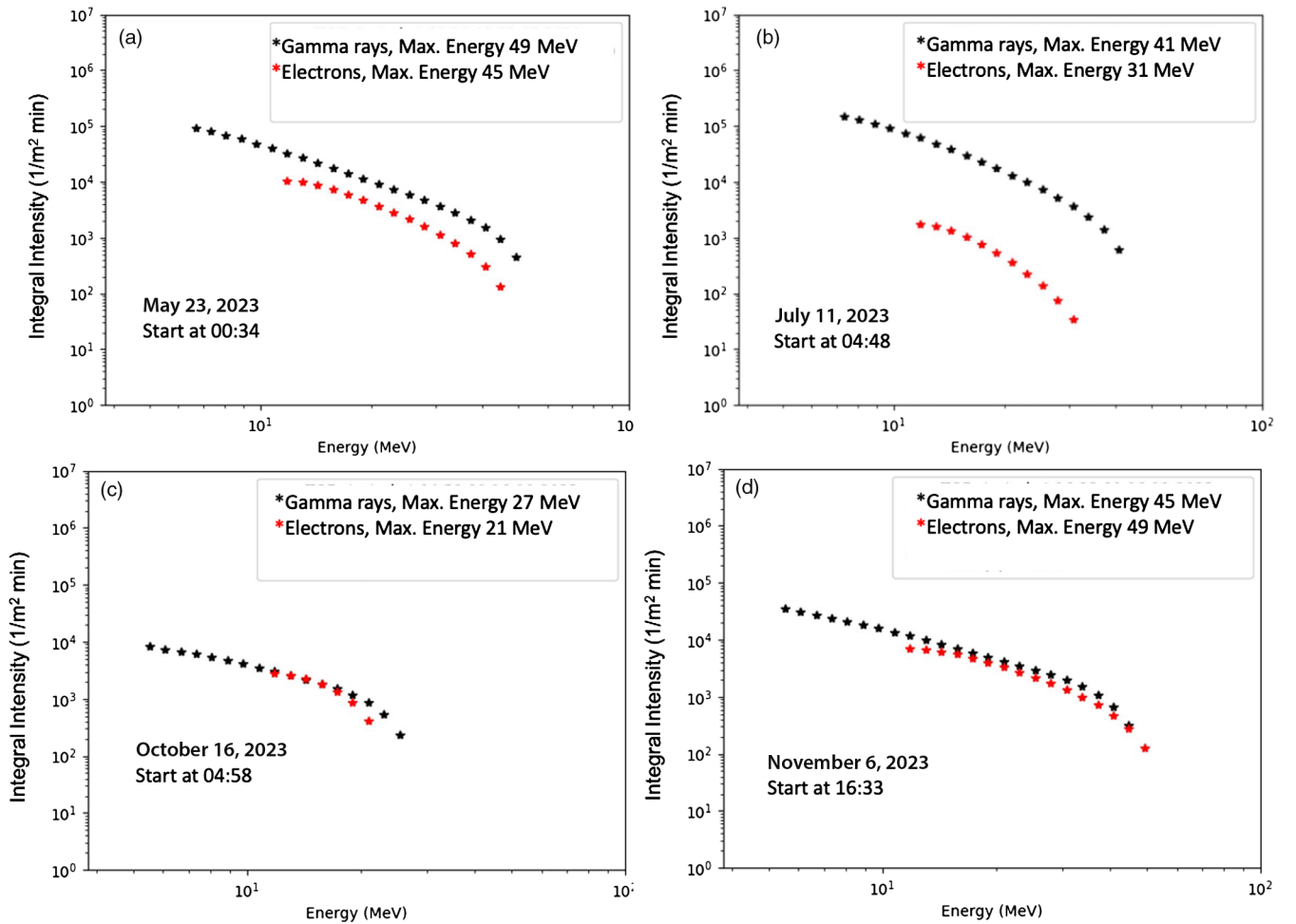
FIG. 7.   The integral energy spectra of the largest TGEs of 2023. (a) May 23, (b) July 11, (c) October 16, and (d) November 6.

standard and relative errors, the enhancement in percent, and its significance in the number of standard deviations above the mean value measured at fair weather. We also present the equivalent significance for the 1-minute time series for comparative purposes.

As shown in Figs. 6(a)–6(d), the TGE flux is very stable—the relative errors for all four TGEs are smaller than the ones calculated for the ambient cosmic ray flux (a day earlier). Thus, despite the fast-changing atmosphere environments, electron accelerators sustain stable particle flux over at least 50000 m^2 (the area covered by the STAND1 network).

Figures 7(a)–7(d) present the integral energy spectra of the four largest TGEs. We estimate energy spectra using a variety of methods. Detectors' count rates with different energy thresholds were initially used to obtain energy-release histograms [30]. Energy spectra are then further refined by solving the inverse problem using detailed calculation of the ASNT detector response function with the GEANT4 package [31]. The energy spectra presented in Fig. 7 were recovered from the energy release histograms measured by the CUBE detector. We use two 20 cm thick

and 0.25 m^2 area plastic scintillators for spectrometry and a 1 cm thick and 1 m^2 area scintillator fully covering spectrometric scintillators for vetoing charged fluxes. Using coincidences of two scintillators, we isolate charged and neutral fluxes. The logarithmic amplitude-digit converter, used in the CUBE detector, allows measurement of the energy deposits in a wide dynamic range of input signal amplitudes (corresponding to particle energies from 0.3 to 100 MeV).

The energy spectra of electrons and gamma rays during Autumn TGEs [see Figs. 7(c) and 7(d)] are very similar, unlike the summer TGEs [Fig. 7(b)], which are very different. Comparing electron and gamma-ray energy spectra allows for estimating the location of the AEF. This specific issue will be explored in the next section.

V. FREE PASSAGE DISTANCE AND DISTANCE TO THE CLOUD BASE

The location of the AEF is estimated using several parameters calculated from the initial measurements. These parameters include the distance to the cloud base

and the free passage distance (FPD) from the ground where the RREA avalanche leaves the AEF. The FPD is calculated using an empirical equation (1) confirmed by simulations [32],

$$FPD(\text{meters}) = (C_1 * E_{max}^{\gamma} - E_{max}^{e})/C_2 \qquad (1)$$

Coefficients C_1 and C_2 are estimated to be 1.2 and 0.2, respectively. TGE simulations suggest that the maximum energy of electrons going out of the electric field is 20% higher than that of gamma rays. Therefore, we can estimate the maximum energy of electrons leaving the field by $C_1 * E^{\gamma}$ max. Furthermore, we assume that the maximum energy of gamma rays does not change significantly when they travel 100 m or less in the atmosphere. Also, we assume that electrons lose approximately 0.2 MeV per m at altitudes of about 3000 m. We conducted multiple simulations of electron-gamma ray avalanches in the atmosphere to verify the accuracy of Eq. (1) and detect any potential methodological errors. We utilize CORSIKA simulations [33] with varying electric field strengths and locations to achieve this. We store the particle energies reaching the ground and solve the inverse problem to recover the AEF strength and location from the measured TGE. Subsequently, we apply all experimental procedures to the obtained samples to estimate the maximum energies of electrons and gamma rays ([32], supplemented

materials). Once we have calculated the FPD parameter, we compare it to the "true" value in the simulation. Based on this comparison, we estimate the method's standard error to be ≈50 meters.

The cloud base height is recovered by calculating the temperature and dew point according to the well-known approximate Eq. (2) [34]. The difference (spread) between the air temperature and the dew point indicates how much cooling is needed for condensation. This method assumes a linear and uniform decrease in temperature with altitude, which might not always be the case in real atmospheric conditions with local variations.

$$H(m) \approx (\text{Air temperature at surface}\{°C\}$$
$$- \text{dew point temperature}\{°C\}) \times 122 \qquad (2)$$

The FPD and cloud base are posted in Table 1. Table 1 also displays TGE significances in percent relative to fair weather flux, TGE duration, and weather parameters. The third to fifth columns show the percentage of TGE enhancement of STAND3's "1000" coincidence and absolute count rate enhancement of coincidences "1100" and "1110" targeting high-energy electrons; the sixth column shows the percentage of enhancement of SEVAN detectors "100" coincidence; seventh column—TGE duration by the STAND3's "1000" coincidence; eighth column—outside temperature. The ninth and tenth columns show the

TABLE I. Detailed information on the 18 largest TGEs of 2023. The count rate significance was calculated using STAND3 with a "1000" coincidence. TGEs with an enhancement of more than 75% are denoted in bold.

| Date	Time (UT)	STAND3 coincidence 1000 (%)	Coincidence 1100 count	Coincidence 1110 count	SEVAN coincidence 100 (%)	Duration (min)	Temperature (C°)	Cloud base (m)	FPD (m)	EFM (km)
April 4, 2023	02:08	36	867	450	6.0	7	−4.7	61		17.0
April 19, 2023	15:27	49	1200	432	7.0	8	−1.8	49		3.0
May 8, 2023	02:02	28	729	287	3.9	26	−1.9	73		17.0
May 18, 2023	05:19	26	553	240	6.4	8	1.9	232		7.0
May 23, 2023	**00:31**	**675**	**4020**	**1080**	**69.7**	**5**	**0.1**	**37**	**70**	**3.0**
May 27, 2023	**15:10**	**75**	**1400**	**650**	**15.5**	**32**	**0.5**	**73**	**57**	**14.0**
May 31, 2023	08:35	30	657	237	13.4	13	1.1	122		4.0
June 22, 2023	08:18	21	387	180	7.3	30	1.6	73		16.0
June 23, 2023	03:48	41	646	313	18.0	13	2.0	97		20.0
June 23, 2023	05:08	32	568	184	10.2	17	3.1	97		12.0
June 24, 2023	08:31	21	360	250	7.6	14	4.8	37		2.0
July 11, 2023	**04:45**	**261**	**900**	**200**	**70.7**	**7**	**4.1**	**61**	**45**	**18.0**
August 5, 2023	**00:38**	**115.0**	**660**	**22**	**34.4**	**6**	**7.7**	**171**	**215**	**6.0**
September 9, 2023	05:23	22	470	270	9.4	6	3.2	85		14.0
September 25, 2023	**13:41**	**87**	**750**	**400**	**38.7**	**14**	**3.2**	**170**	**115**	**22.0**
October 16, 2023	**04:57**	**131**	**1530**	**500**	**25.2**	**10**	**−0.6**	**61**	**57**	**3.0**
October 17, 2023	20:19	30	563	274	7.8	15	−0.8	85		18.0
November 6, 2023	**16:33**	**234**	**2500**	**798**	**37.7**	**10**	**1.1**	**97.6**	**25**	**14.0**
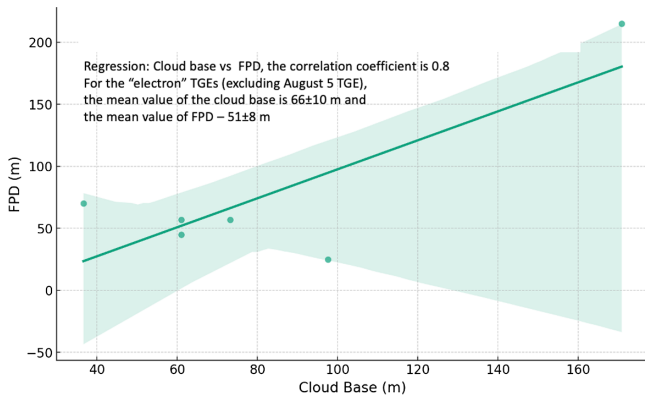
FIG. 8. Dependence of the distance to cloud base from the ground estimated by spread [Eq. 2] on free path distance estimated by Eq. (1).

cloud base height and free passage distance, estimated by Eqs. (1) and (2). The last column shows the distance to the nearest lightning flash during TGE. By the bold fonts, we denote the five largest TGEs; those count rates exceed 75% of fair weather. We use the coincidences of the STAND3 detector to emphasize the electron content of the Spring and Autumn events and the scarcity of electrons in summer TGEs.

Table 1 shows that four of the seven largest TGEs occurred during the night or early morning, whereas three occurred in the afternoon. Additionally, three of the largest TGEs were terminated by a lightning flash. The number of electrons selected by coincidences of the STAND3 detector indicates the presence of electrons in TGE flux. On May 23

and November 6, the number of particles selected by the "1110" coincidence (electrons with energies above 30 MeV) was 1080 and 798, respectively, which well agrees with the integral energy spectra [Figs. 7(a) and 7(d)]. The low location of cloud base height, measured TGE intensities, and recovered energy spectra indicate that a strong electric field with a strength of at least 2.1 kV/cm can be present 50 m above ground. 2.1 kV/cm is the minimal strength of the electric field, which can sustain the RREA process at a height of 3250 m [32].

Figure 8 presents the regression function of the free path distance (FPD) and the distance to the cloud base for the largest TGEs. While they are expected to be correlated, the relationship shown in Fig. 8 provides the first direct evidence. The five largest TGEs occurred when both FPD and distance to the cloud base were less than a hundred meters, and for all of them, the recovered energy spectrum of TGE electrons was similar to the gamma-ray spectrum. Despite the spectrometers being located under the roof of the SKL building, we obtain TGE particle energy spectra above the roof by a full GEANT4 simulation of particle transport through the building and detector materials.

At energies above 50 MeV, the MOS (modification of electron spectra) effect can also play a role [35]. MOS process results in enhancement of the bremsstrahlung gamma rays by a few shares of a percent and, at low energies, is negligible. However, due to weak fluxes and small spectrometer areas, it can contaminate TGE flux at the highest energies. Therefore, we estimate the energy of TGE electrons in the most intensive to be ≈50 MeV.
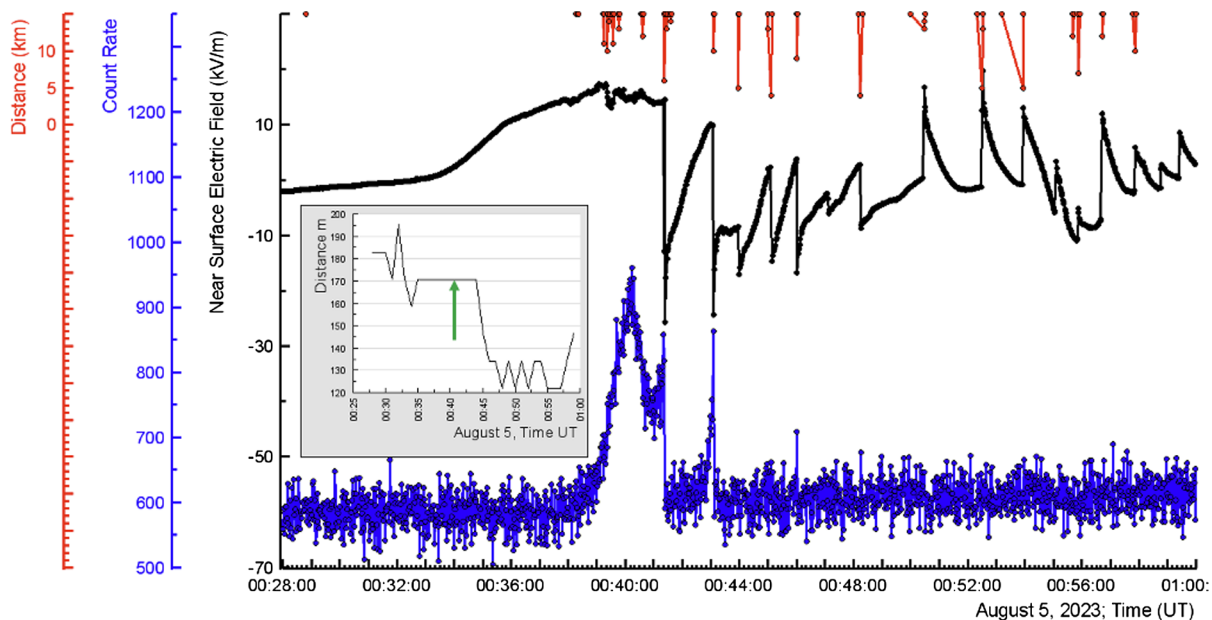

FIG. 9. The time series of STAND1's upper scintillator (blue) abruptly terminated by lightning flashes, disturbances of NSEF (black), and distances to the lightning flash (red). The inset shows the time series of distances to the cloud base.
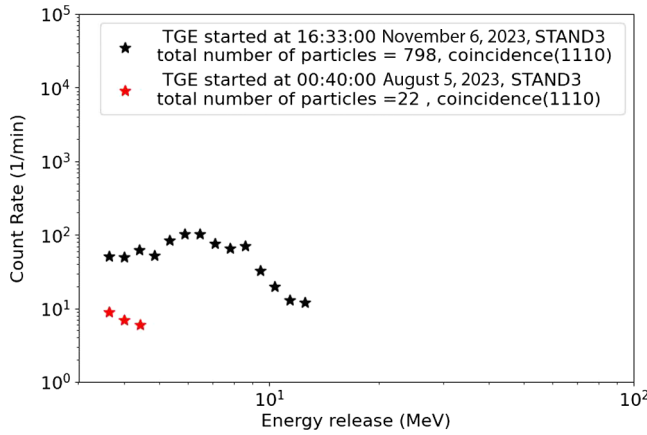
FIG. 10.   The energy release histograms of TGE electrons in a 3 cm thick upper scintillator of STAND3 detector.

VI. FURTHER ANALYSIS OF TGE DATA

We have created an open-access database to make TGE data accessible to the community. In support of this effort, we have gathered summary information and stored it in the Mendeley datasets, along with detailed explanations [3]. The Excel table is accompanied by figures presenting 56 TGE events. It provides direct links to the corresponding graphical representations in the Cosmic Ray Division (CRD) database of the Yerevan Physics Institute (ADEI, [15,36]), offering extensive multivariate visualization and statistical analysis capabilities.

We aim to provide extensive multivariate data for researchers to analyze potential correlations between charged and neutral particle fluxes, electric field strengths, lightning occurrences, and meteorological parameters. This is achieved by combining the ADEI visualization and correlation analysis platform with the Excel files found in the Mendeley datasets. Below, we showcase examples of further analysis of TGE data using the ADEI platform.

In Fig. 9, we show the TGE occurred on August 5 by STAND1's upper scintillator count rate. As we already discussed, the cloud height and FDP for this event were large (see Table 1 and inset to Fig. 9). The intensity of electron flux was very low (the intensity of "1111" coincidence of the STAND3 detector was 0 and of "1110" only 22). The estimated cloud base height was 170 m; correspondingly, the electron flux attenuated; mostly gamma rays reached the detector. The lightning activity was very high during the event. Flashes interrupted the TGE several times at 00:41:23, 00:43:05, 00:43:57, 00:45:05, etc. Afterward, the "charging engine" reoperated the lower dipole, and particle flux started rising till another flash grounded the potential difference.

In Fig. 10, we show the electron energy release histograms in the 3 cm thick scintillator of the STAND3 detector. The energy releases correspond to the "1110" trigger condition, i.e., selecting electrons with energies >30 MeV. During the TGE of 5 August, when the strength of AEF decayed at ≈200 m above ground, only 22 low-energy electrons were registered. In contrast, on 6 November, when the distance was well below 100 m, 798 electrons were registered. This relation agrees with our estimates based on the modeling of RREA propagation in 200 and 25 m of air; see [37,38].

Figure 11 shows a remarkable event with an exceptionally long duration and a significant intensity. The TGE
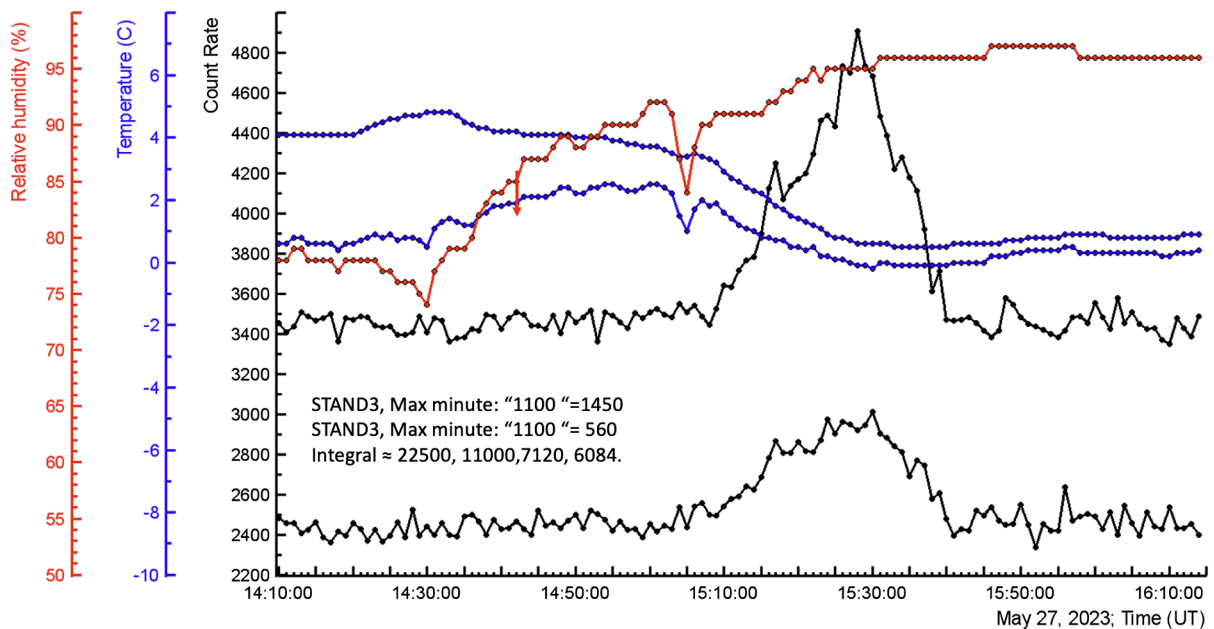

FIG. 11.   1-minute time series of STAND's "1100" coincidence (upper black) and "1110" coincidence (lower black); blue curves—temperature and dew point; red—relative humidity.
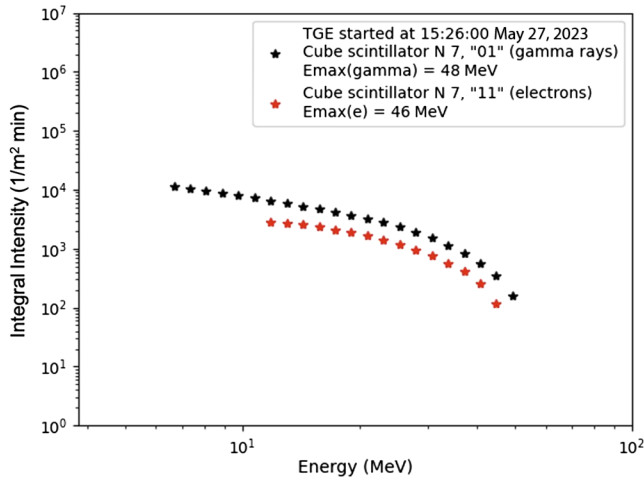
FIG. 12. The integral energy spectra of gamma rays (black) and electrons (red) recovered by the CUBE spectrometer.

FIG. 14. Scatter plot between the distances to the lightning flash and their duration for 2023 TGEs, those that abruptly ended by flash (in red, 22 flashes) and those that smoothly finished (in green, 34 flashes). The dashed line divides two classes of events: terminated by flash to the left and smoothly finished to the right.

lasted 32 minutes, with no lightning flash detected within 10 km, and ended smoothly. The fluence of the event was very high, ≈ 38 particles/cm^2 for energies above 1 MeV. The outside temperature and humidity were stable during TGE. In the body of the plot, we show the maximum count rates of two coincidences and the total count rate (integral) of the whole TGE for all coincidences.

The CUBE spectrometer measured maximum energies of 48 MeV for TGE gamma rays and 46 MeV for electrons (Fig. 12). The extension of AEF near the ground is confirmed by the large intensity of STAND's coincidence "1110," as shown in Fig. 12. The FPD calculated by Eq. (1) is approximately 70 m, which is in good agreement with the estimate of the cloud base height by Eq. (2) (57 m).

As we see in Fig. 13, from 18 large TGEs (>20% enhancement, see Table 1) occurred at night-morning of the day. The monthly distribution outlines May and June as the most frequent months for TGE occurrence (9 from 18).

In Fig. 14, a scatter plot shows the relationship between the distance to the nearest lightning flash and TGE
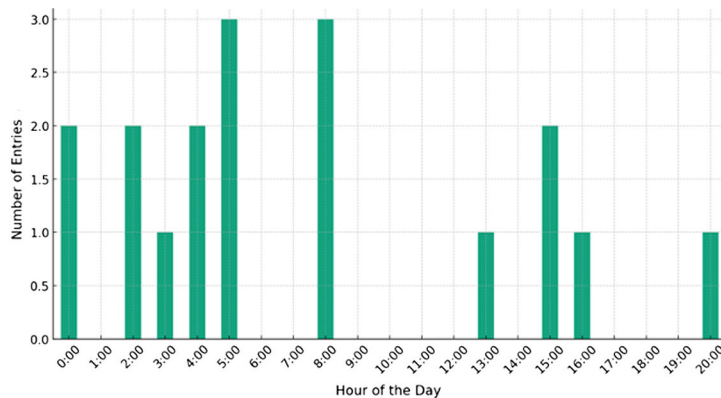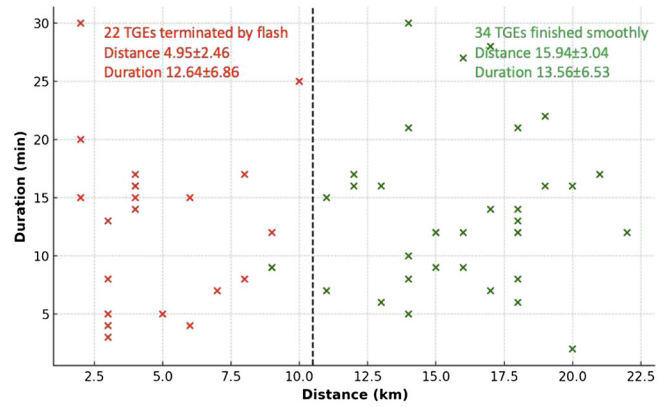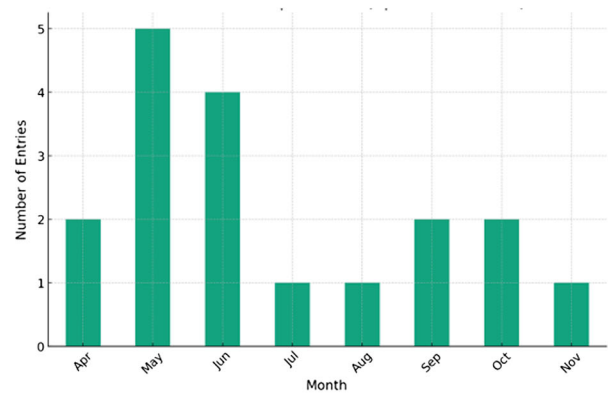
duration. The plot indicates that TGEs can only be terminated by lightning flashes less than 10 km away, shown in red. This distance is typical for convective cells within a thunderstorm. If no nearby flashes were detected, TGEs ended smoothly. Two classes are well separated; only one TGE that ended smoothly was misclassified if the decision line was set at 10 km (indicated by the dashed line in the plot). The mean distances for red and green classes, 4.95 km and 15.94 km, are separated by 4σ. The distribution of the TGE duration for both classes did not differ significantly. Therefore, lightning flashes can terminate TGEs at all stages of development, as illustrated in Fig. 9, where multiple lightning flashes terminate TGEs at different phases of development.

Observations of lightning-terminated TGEs, like those included in Fig. 14, may be relevant to lightning initiation by RREA [39]. While only a small fraction of detected lightning strikes are associated with a detected TGE, TGE detection is only possible when the RREA occurs over the detector network at a suitably low altitude. Thus, the

FIG. 13. Daily and monthly distributions of the TGEs registered in 2023 (largest TGEs with enhancement > 20% according to STAND3's "1000" coincidence).

number of lightning flashes associated with RREA is likely much higher, and RREA may be an important precursor to lightning flashes.

VII. CONCLUSIONS

(i) Based on the thunderstorm ground enhancements (TGEs) recorded in 2023, we substantiate that extensive electric fields catalyze relativistic runaway electron avalanches (RREAs) in extensive regions within thunderclouds. These RREAs generate TGEs that cover multiple square kilometers on the Earth's surface.

(ii) We have observed a seasonal and diurnal pattern in TGE occurrences, with a higher frequency during May and June and predominantly in the night-to-morning hours.

(iii) The most intense TGE event above Aragats exhibited a tenfold increase in particle flux intensity, with TGE electron energies surging up to 60 MeV. Concurrently, the maximum TGE fluence was measured at 38 particles per square centimeter.

(iv) Our research indicates that atmospheric electric fields associated with TGEs with large electron content can be as strong as 2.1 kV/cm and present as low as 50 meters above the ground.

(v) Despite the chaotic nature of atmospheric electric fields, electron accelerators within thunderclouds demonstrated remarkable stability, maintaining a steady flux for durations of 0.5 to 2 minutes. The relative error of TGE flux at these minutes was lower than that associated with the ambient cosmic ray population, indicating a high level of stability of the electron accelerator. This finding indicates a level of organization within the atmospheric electric fields that was previously unappreciated.

(vi) There were no lightning flashes during most of the observed TGEs (34 out of 56), detected within 10 km of the detectors.

(vii) We introduce two interrelated empiric parameters, free passage distance, and cloud base height, to characterize the location of the vertical atmospheric electric field. These parameters are well correlated with the measured intensity of the TGE fluxes.

(viii) Monitoring the maximum energy of the electron flux during thunderstorms with a simple spectrometer can be useful for alerting on extreme near-surface electric fields that can be dangerous during rocket launch and charging.

The data underpinning this study can be accessed in numerical and graphical formats through the multivariate visualization software platform ADEI, hosted on the Cosmic Ray Division (CRD) webpage of the Yerevan Physics Institute [36].

[1] A. Chilingarian, A. Daryan, K. Arakelyan, A. Hovhannisyan, B. Mailyan, L. Melkumyan, G. Hovsepyan, S. Chilingaryan, A. Reymers, and L. Vanyan, Ground-based observations of thunderstorm-correlated fluxes of high-energy electrons, gamma rays, and neutrons, Phys. Rev. D **82**, 043009 (2010).

[2] A. Chilingarian, G. Hovsepyan, and A. Hovhannisyan, Particle bursts from thunderclouds: Natural particle accelerators above our heads, Phys. Rev. D **83**, 062001 (2011).

[3] A. Chilingarian, T. Karapetyan, D. Aslanyan, and B. Sargsyan, Extreme thunderstorm ground enhancements registered on Aragats in 2023, Mendeley Data **V1** (2024), 10.17632/z4ry54hccb.1.

[4] A. Chilingarian, D. Pokhsraryan, F. Zagumennov, and M. Zazyan, Space-temporal structure of the thunderstorm ground enhancements (TGEs), Phys. Open **18**, 100202 (2024).

[5] A. V. Gurevich, G. M. Milikh, and R. A. Roussel-Dupre, Runaway electron mechanism of air breakdown and preconditioning during a thunderstorm, Phys. Lett. A **165**, 463 (1992).

[6] A. Chilingarian, N. Bostanjyan, T. Karapetyan, and L. Vanyan, Remarks on recent results on neutron production during thunderstorms, Phys. Rev. D **86**, 093017 (2012).

[7] J. R. Dwyer, A fundamental limit on electric fields in air, Geophys. Res. Lett. **30**, 2055 (2003).

[8] L. P. Babich, E. N. Donskoy, R. I. Il'kaev, I. M. Kutsyk, and R. A. Roussel-Dupre, Fundamental parameters of a relativistic runaway electron avalanche in air, Plasma Phys. Rep. **30**, 616 (2004).

[9] J. Chum, R. Langer, J. Baše, M. Kollárik, I. Strhárský, G. Diendorfer, and J. Rusz, Significant enhancements of secondary cosmic rays and electric field at high mountain peak during thunderstorms, Earth Planets Space **72**, 28 (2020).

[10] A. Chilingarian, G. Hovsepyan, S. Kazaryan *et al.*, Correlated measurements of secondary cosmic ray fluxes by the Aragats space- environmental center monitors, Nucl. Instrum. Methods Phys. Res., Sect. A **543**, 483 (2005).

[11] A. Chilingarian, G. Hovsepyan, D. Aslanyan *et al.*, Thunderstorm ground enhancements: Multivariate analysis of 12 years of observations, Phys. Rev. D **106**, 082004 (2022).

[12] A. Chilingarian, G. Hovsepyan, D. Aslanyan, B. Sargsyan, and T. Karapetyan, Catalog of Thunderstorm Ground Enhancements (TGEs) observed at Aragats in 2013–2021, Mendeley Data **V1** (2022), 10.17632/8gtdbch59z.1.

[13] A. Chilingarian, G. Hovsepyan, T. Karapetyan, B. Sargsyan, and E. Svechnikova, Transient luminous events in the lower part of the atmosphere originated in the peripheral regions of a thunderstorm , Universe **8**, 412 (2022).

[14] J. R. Dwyer, D. M. Smith, and S. A. Cummer, High-energy atmospheric physics: Terrestrial gamma-ray flashes and related phenomena, Space Sci. Rev. **173**, 133 (2012).

[15] S. Chilingaryan, A. Chilingarian, V. Danielyan, and W. Eppler, The Aragats data acquisition system for highly distributed particle detecting networks, J. Phys. Conf. Ser. **119**, 082001 (2008).

[16] A. Chilingarian, T. Karapetyan, Y. Khanikyanc, and S. Chilingaryan, Measurements of particle fluxes, electric fields, and lightning occurrences at the Aragats Space-Environmental Center (ASEC). Pure Appl. Geophys. **181**, 1963 (2024).

[17] BOLTEK, available online: https://www.boltek.com/EFM-100C_Manual_030323.pdf (accessed on 1 August 2024).

[18] DAVIS Weather Station, available online: https://www.davisweatherstation.com/ (accessed on 1 July 2024).

[19] A. Chilingarian, G. Hovsepyan, T. Karapetyan, B. Sarsyan, and S. Chilingaryan, Measurements of energy spectra of relativistic electrons and gamma-rays avalanches developed in the thunderous atmosphere with Aragats Solar Neutron Telescope, J. Instrum. **17**, P03002 (2022).

[20] A. Chilingarian, T. Karapetyan, B. Sargsyan, J. Knapp, M. Walter, and T. Rehm, Energy spectra of the first TGE observed on Zugspitze by the SEVAN light detector compared with the energetic TGE observed on Aragats, Astropart. Phys. **156**, 102924 (2024).

[21] T. V. Danilova, E. A. Danilova, and A. B. Erlikin, The ANI experiment: On the investigation of interactions from hadrons and nuclei in the energy range 10^3–10^5 TeV, Nucl. Instrum. Methods Phys. Res., Sect. A **323**, 104 (1992).

[22] N. K. Bostanjyan, A. Chilingarian, V. Eganov, and G. Karapetyan, On the production of highest energy solar protons at 20 January 2005, J. Adv. Space Res. **39**, 1454 (2007).

[23] A. Chilingarian and G. Hovsepyan, Proving "new physics" by measuring cosmic ray fluxes, Astron. Comput. **44**, 100714 (2023).

[24] A. Chilingarian, G. Hovsepyan, T. Karapetyan, L. Kozliner, S. Chilingaryan, D. Pokhsraryan, and B. Sargsyan, The horizontal profile of the atmospheric electric fields as measured during thunderstorms by the network of NaI spectrometers located on the slopes of Mt. Aragats, J. Instrum. **17**, P10011 (2022).

[25] N. Ostgaard, T. G. Lang, M. Marisaldi *et al.*, Results from the ALOFT mission: A flight campaign for TGF and gamma-ray glow observations over Central America and the Caribbean in July 2023, AE22A-03 (AGU, San Francisco, 2023), 10.5194/egusphere-egu23-3116.

[26] A. Chilingarian and B. Sargsyan, Atmospheric positron flux modulation during thunderstorms, Phys. Rev. D **109**, 062003 (2024).

[27] A. Chilingarian, B. Sargsyan, and M. Zazyan, An enormous increase in atmospheric positron flux during a summer thunderstorm on Mount Aragats, Radiat. Phys. Chem. **222**, 111819 (2024).

[28] A. Chilingarian, Y. Khanikyants, V. A. Rakov, and S. Soghomonyan, Termination of thunderstorm-related bursts of energetic radiation and particles by inverted-polarity intracloud and hybrid lightning discharge, Atmos. Res. **233**, 104713 (2020).

[29] A. Chilingarian, Y. Khanikyants, and V. Rakov, Corrigendum to "Termination of thunderstorm-related bursts of energetic radiation and particles by inverted intracloud and hybrid lightning discharges" [Atmospheric Research, 233 (2020), 104713–104720], Atmos. Res. **304**, 107403 (2024)..

[30] A. Chilingarian, B. Mailyan, and L. Vanyan, Observation of Thunderstorm Ground Enhancements with intense fluxes of high-energy electrons, Astropart. Phys. **48**, 1 (2013).

[31] S. Agostinelli, J. Allison, K. Amako *et al.*, Geant4—A simulation toolkit, Nucl. Instrum. Methods Phys. Res., Sect. A **506**, 250 (2003).

[32] A. Chilingarian, G. Hovsepyan, and M. Zazyan, Measurement of TGE particle energy spectra: An insight in the cloud charge structure, Europhys. Lett. **134**, 69001 (2021).

[33] D. Heck, J. Knapp, J. N. Capdevielle, G. Schatz, and T. Thouw, Forschungszentrum (Nuclear Research Center), Karlsruhe, Report No. FZKA 6019, 1998, https://www.ikp.kit.edu/corsika/70.php.

[34] CLOUD BASE, the online calculator: https://www.omnicalculator.com/physics/cloud-base (accessed on 1 July 2024).

[35] A. Chilingarian, B. Mailyan, and L. Vanyan, Recovering the energy spectra of electrons and gamma rays coming from the thunderclouds, Atmos. Res. **114–115**, 1 (2012).

[36] ADEI, available online: http://adei.crd.yerphi.am/ (accessed on 1 August 2024).

[37] A. Chilingarian, G. Hovsepyan, D. Aslanyan, T. Karapetyan, B. Sargsyan, and M. Zazyan, TGE electron energy spectra: Comment on "Radar diagnosis of the thundercloud electron accelerator" by E. Williams et al. (2022), J. Geophys. Res. Atmos. **128**, e2022JD037309 (2023).

[38] E. Williams, B. Mailyan, G. Karapetyan, and R. Mkrtchyan, Conditions for energetic electrons and gamma rays in thunderstorm ground enhancements, J. Geophys. Res. Atmos. **128**, e2023JD039612 (2023).

[39] A. Chilingarian, S. Chilingaryan, T. Karapetyan, L. Kozliner, Y. Khanikyants, G. Hovsepyan, D. Pokhsraryan, and S. Soghomonyan, On the initiation of lightning in thunderclouds, Sci. Rep. **7**, 1371 (2017).